The Effect of Magnesium Ions on Triphosphate Hydrolysis

Alexandre Barrozo[1], David Blaha-Nelson[2], N. H. Williams[3,*] and S. C. L. Kamerlin[2,*]

[1.] University of Southern California, Department of Chemistry, Los Angeles CA 90089-1062, USA.
[2.] Department of Cell and Molecular Biology, Uppsala University, BMC Box 596, S-751 24 Uppsala, Sweden.[3.] Department of Chemistry, Sheffield University, Sheffield S3 7HF, UK.

Corresponding author email addresses: n.h.williams@sheffield.ac.uk, kamerlin@icm.uu.se

Abstract

The role of metal ions in catalyzing phosphate ester hydrolysis has been the subject of much debate, both in terms of whether they change the transition state structure or mechanistic pathway. Understanding the impact of metal ions on these biologically critical reactions is central to improving our understanding of the role of metal ions in the numerous enzymes that facilitate them. In the present study, we have performed density functional theory studies of the mechanisms of methyl triphosphate and acetyl phosphate hydrolysis in aqueous solution to explore the competition between solvent- and substrate-assisted pathways, and examined the impact of Mg^{2+} on the energetics and transition state geometries. In both cases, we observe a clear preference for a more dissociative solvent-assisted transition state, which is not significantly changed by coordination of Mg^{2+}. The effect of Mg^{2+} on the transition state geometries for the two pathways is minimal. While our calculations cannot rule out a substrate-assisted pathway as a possible solution for biological phosphate hydrolysis, they demonstrate that a significantly higher energy barrier needs to be overcome in the enzymatic reaction for this to be an energetically viable reaction pathway.

Keywords: methyl triphosphate • acetyl phosphate • density functional theory • phosphate hydrolysis • metals in biology

Introduction

Phosphate esters are the building blocks of life, and are involved in facilitating all cellular processes, from cellular signaling to protein synthesis [1, 2]. Due to this, the enzymes that regulate these reactions are major drug targets [3-5], and understanding their mechanisms has been the subject of substantial experimental and computational effort (for reviews, see *e.g.* refs. [1, 6, 7], and references cited therein). The mechanisms of these reactions and the importance of the different factors affecting the fundamental mechanistic preferences (such as environment or leaving/spectator group effects) have been hotly debated [6, 7], without reaching a mechanistic consensus. For example, in the case of GTP hydrolysis by GTPases such as Ras GTPase, arguments have been put forward in favour of phosphorane intermediates and concerted reaction pathways [8], of substrate assisted-catalysis [9-13], of general base catalysis with the involvement of active site residues [14-17], or the possibility that no deprotonation of the nucleophile is required to drive the reaction [6, 18]. A similar lack of mechanistic clarity exists for many other enzymes that catalyze phosphoryl transfer

reactions (see discussion in *e.g.* ref. [7], among many others), creating barriers to further progress in our understanding of the factors that shape structure-function-activity relationships in these system, as well as how they can be manipulated, for instance for therapeutic purposes.

To resolve these mechanistic ambiguities with respect to biologically catalysed phosphoryl transfer, it is essential to first obtain a thorough understanding of the intrinsic mechanisms of the corresponding uncatalyzed reactions, and the factors affecting the choice of mechanism for phosphate esters with different leaving groups. Here, once again, computational studies have provided varied interpretations, depending on the precise approach and level of theory used, suggesting a range of mechanisms running the full spectrum from fully associative (A_N+D_N) to fully dissociative (D_N+A_N) pathways, as well as concerted (A_ND_N) pathways without intermediates (see discussion in refs. [7, 8] and references cited therein). To partially address this issue, we recently performed detailed comparisons of a range of phosphate monoester dianions with different leaving groups, examining both leaving group effects and the effect of including explicit microsolvation in the calculations [19, 20]. In addition to reasonable quantitative agreement between experimental and calculated activation free energies, our calculations reproduced both the linear free energy relationship for phosphate monoester dianion hydrolysis, as well as the experimentally observed kinetic isotope effects for *p*-nitrophenyl phosphate hydrolysis [19]. These calculations demonstrated a clear preference for a solvent assisted pathway for phosphate monoesters with good leaving groups, while hinting at a potential transition to a substrate-assisted pathway for compounds with poor leaving groups, although this would only happen for leaving groups with quite high pK_as (previous work suggested a crossover at a leaving group pK_a of ~13). This predicted mechanistic preference is in good agreement with experimental considerations of kinetic isotope effects, entropic effects and linear free energy relationships for phosphate monoester dianion hydrolysis [21-24], all of which have been traditionally interpreted as pointing to a reaction proceeding through a concerted pathway with a loose, dissociative transition state.

An additional complication in transferring these insights to biologically catalyzed reactions is that metal ions often play crucial roles in enzyme-catalyzed reactions, for example by acting as Lewis acids, or by modulating the pK_as of active site nucleophiles. Metal ions have been linked to changes in substrate-preference in enzyme-catalyzed reactions, and also have been suggested to play an important role in the emergence of new enzyme functions [25, 26]. Most significantly for mechanistic investigations, it has often been speculated that their

Lewis acidity may change the mechanism, or the character of the reaction, favouring more associative pathways where the positive charge density would have a role in stabilizing the high-energy states. Therefore, in the present work, we have explored the role of magnesium ions on the mechanistic preferences of phosphate monoester hydrolysis, using acetyl phosphate and methyl triphosphate as model systems (based on the experimental data available on the hydrolysis of acetyl phosphate [27-33], ATP [34] and GTP [35]).

Admiraal and Herschlag have examined in detail the kinetics of phosphoryl transfer from GTP, ATP and a series of pyrophosphates to a series of alcohols [34]. They obtained a small Brønsted β_{nuc} value (0.07), suggesting the presence of a transition state with little bond formation between the incoming nucleophile and the phosphate. This was complemented by examining the β_{lg} value for phosphoryl transfer to water from a series of phosphoanhydrides, which yielded a large a large and negative value (-1.1) supporting a largely dissociative transition state in which bond cleavage to the leaving group is advanced at the transition state. Interestingly, the inclusion of Mg^{2+} ions had minimal effect on the β_{nuc} value, or on the reaction rates, for instance only reducing the activation barrier for ATP hydrolysis by 0.7 $kcal \cdot mol^{-1}$ at 60 °C. Kötting and Gerwert studied the hydrolysis of GTP over a range of temperatures, in the presence and absence of Mg^{2+} [35]. Consistent with Admiraal and Herschlag's data, they found that the difference in activation energy was minimal: at 25 °C, there is no observed difference in rate (with an experimental activation energy of 27.9 $kcal \cdot mol^{-1}$). The presence of Mg^{2+} did accelerate the reaction at higher temperatures due to a higher enthalpy of activation. Therefore, curiously, inclusion of the magnesium ion appeared to have minimal effect on stabilizing either the transition state or on perturbing the transition state geometry, raising questions about its role in enzyme-catalyzed GTP or ATP hydrolysis.

Following from this, there have been a number of recent different computational studies of GTP, ATP and methyl triphosphate hydrolysis in aqueous solution [36-43], exploring preferred mechanistic options and, where metal ions have been included, the potential roles of the metal ion. Interestingly, some of these studies have provided quite contradictory mechanistic interpretations depending on the precise level of theory used and how the simulations were set up, making it hard to reach any concrete mechanistic conclusions. In addition, the calculated activation free energies in refs. [36, 38-40, 42, 43] were often (but not always [37, 41]) far higher than those measured experimentally.

Therefore, in the present work, we have used methyl triphosphate (MeTP) hydrolysis as a model system, and considered the effect of a single magnesium ion on both substrate and solvent assisted pathways (**Figure 1**) at the same level of theory, allowing for direct

comparison between the different mechanistic options. We have also carried out the same level of calculations with an analogous study of acetyl phosphate (AcP) hydrolysis, again both with and without bound Mg^{2+}, in order to be able to make a direct link to our previous studies of phosphate monoester dianion hydrolysis [19, 20].

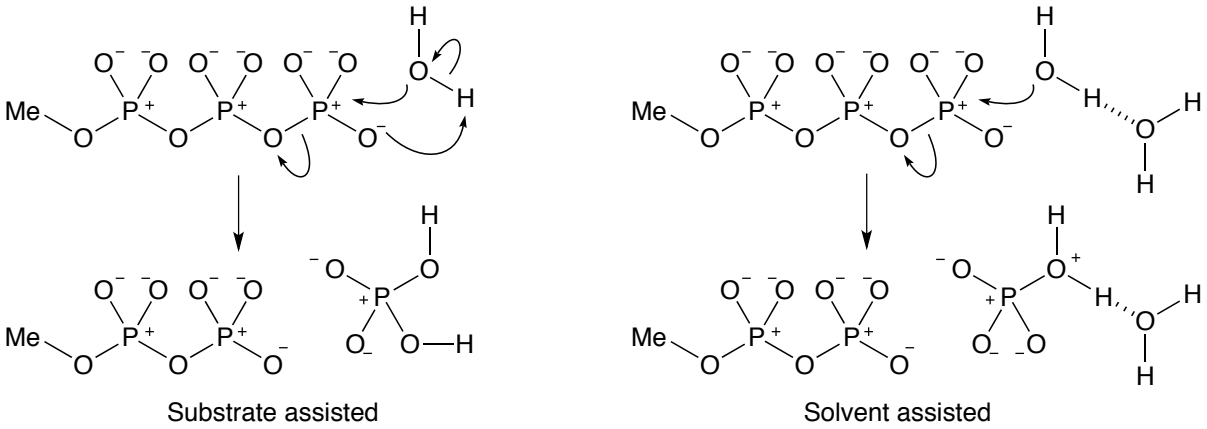

Figure 1: A comparison of (left) substrate- and (right) solvent-assisted pathways for the hydrolysis of methyl triphosphate.

We previously suggested that in the absence of metal ions, the preferred pathway for the hydrolysis of phosphate monoesters with good leaving groups is one involving a loose, dissociative transition state [19, 20]. We demonstrate that for both compounds studied here, the presence of magnesium ions increases the energetic difference between substrate- and solvent-assisted pathways, creating a greater preference for a solvent-assisted pathway than in the absence of the metal. In the case of methyl triphosphate hydrolysis, this occurs irrespectively of the binding mode of the metal ion. In addition, in all cases, the reaction proceeds through a single concerted transition state with no evidence for a phosphorane intermediate.

Methodology

In the present work, we have examined the relative energetics and transition state geometries for the solvent- and substrate-assisted hydrolyses of acetyl phosphate and methyl triphosphate both in the presence and absence of magnesium ions. In the case of methyl triphosphate hydrolysis, we have considered three different binding modes for the magnesium ion (**Figure 2**), such that it is either bridging the α and β phosphates, the β and γ phosphates or all three phosphates at once. As our previous work highlighted the importance of including explicit microsolvation when performing such calculations [19], we have included 8 and 14

water molecules in addition to the nucleophilic water molecule in our calculations of acetyl phosphate and methyl triphosphate respectively, extending this to 15 and 17 water molecules respectively in the presence of the magnesium ion in order to complete the solvation shell of the magnesium ion. The remainder of the solvent was described using an implicit solvent model. As with our previous work, the water molecules were symmetrically placed on the nucleophile and leaving group sides of the phosphate, with additional water molecules placed so as to interact with the oxygen atoms of the α and β phosphates of methyl triphosphate. This allowed us to avoid artifacts introduced into the calculations by performing calculations with such highly charged species in a pure implicit solvation model, and we have previously demonstrated that in the analogous example of methyl phosphate hydrolysis, we can reproduce even high level quantum chemical calculations in full explicit solvent using such a simplified mixed solvent model [19, 44].

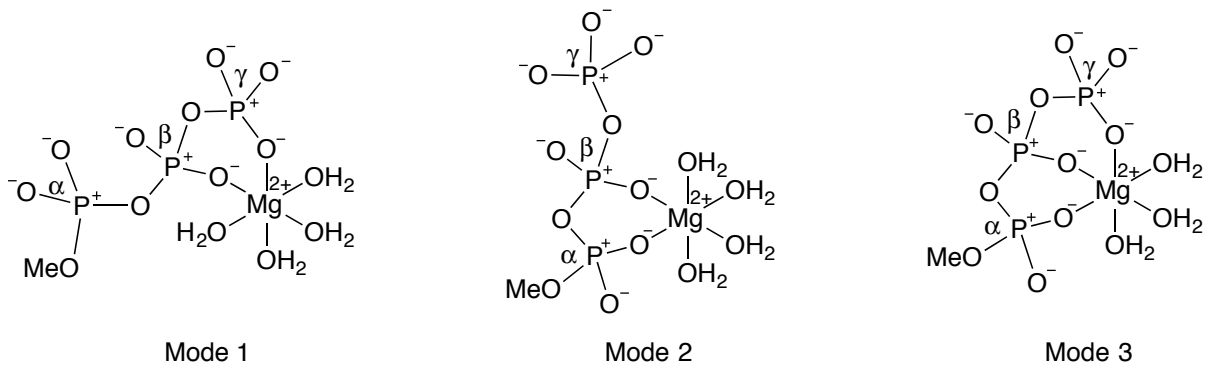

Figure 2: A comparison of the three different Mg^{2+} binding modes to methyl triphosphate considered in this work. In **Mode 1**, the metal ion bridges only the β- and the γ-phosphates, in **Mode 2**, the metal ion bridges only the α- and the β-phosphates, and in **Mode 3**, the metal ion bridges all three phosphates.

All transition states were obtained by structural perturbation of previously optimized transition state geometries for phosphate ester hydrolysis with 8 explicit water molecules [19, 20], with manual addition of magnesium ions and additional water molecules as relevant (see the previous paragraph for the number of water molecules included for each system), as well as partial 1-D scans of the P-O_{nuc} distance to come closer to the saddle point where it was not possible to directly optimize new transition states. The resulting optimized transition states were characterized by means of frequency calculations as well as by following the intrinsic reaction coordinate (IRC) [45, 46] as far as possible in both reactant and product directions, followed by unconstrained geometry optimizations at the same level of theory on the resulting structures to obtain optimized reactant and product states for each reaction pathway, thus

verifying that we are examining the correct transition states for the processes of interest. We note that, as with our previous work [19, 20], our IRC calculations usually led us to a metastable product state rather than the final stable states (in particular in the case of the solvent-assisted pathway). However, as the subsequent changes involve low energy processes and do not affect the difference in energy between the ground state and transition state, we have not focused further on the product states in this work. All calculations were initially performed using the ωB97X-D functional [47] and the 6-31+G(d) basis set, and we then followed this with single point calculations of the electronic energies of the optimized structures using the larger 6-311++G(d,p) basis set, and the vibrational frequencies, zero point energies, and entropies using the same basis set as the geometry optimization (6-31+G(d)). This functional was chosen as it includes corrections for both dispersion and long-range effects. Solvation was accounted for using a mixed solvent model as described above, combining explicit water molecules with the solvent density model (SMD) [48] continuum solvent model. Bond orders were calculated at the same level of theory as the single point calculations, based on the Wiberg bond index [49] using natural bond orbital analysis [50].

Finally, a challenge with performing geometry optimization using mixed explicit/implicit solvent models is the potential dependence of the energetics on the precise orientation of the explicit water molecules included in the system, a problem that is aggravated as more water molecules are explicitly described. In a recent study [19] we demonstrated that in the case of phosphate monoester dianions, while the results are very sensitive to the precise number and orientation of the water molecules when only a smaller number of explicit water molecules are included in the calculations, the more water molecules are explicitly included in the calculations, the less sensitive the calculated energetics become to the precise position of the water molecules.

To ensure that our qualitative results are independent of choice of functional, all obtained transition states were re-optimized using the M11L functional [51], following the same procedure as above, as extra validation of our results. Finally, as IRC calculations with different functionals do not necessarily lead to the same minima, we streamlined our calculations by taking the final optimized reactant and transition states obtained with the M11L functional and then re-optimizing them once again with the ωB97X-D functional. From this ensemble, we selected the lowest energy transition states and ground states to ensure we have been able to obtain a “best available” representation of the structures and energetics for each pathway. While the resulting geometries of the reacting atoms remained largely the same when moving between the different functionals, subtle deviations in the

positions of the water molecules affected the corresponding energetics. To mitigate this issue, we ensured that the positions of the water molecules were as close as possible to each other when comparing solvent- and substrate-assisted transition states for the same system, and had the same pattern of hydrogen bonding interactions. Finally, all transition state energies presented in this work are relative to the energy of the lowest energy ground state for that system obtained from either direct IRC calculations or cross-optimizing structures between functions. This provides a common reference state against which to directly compare all transition state energies for that system. The resulting absolute energies and Cartesian coordinates of each optimized stationary point are provided in the Supporting Information. All calculations were performed using Gaussian09 Rev. E.01 [52].

Results and Discussion

Methyl Triphosphate Hydrolysis

Tables 1 and **2** and **Figure 3** show a comparison of calculated activation free energies for MeTP hydrolysis through solvent- and substrate-assisted pathways, both in the absence and presence of Mg^{2+} ions, calculated using the ωB97X-D and M11L functionals respectively.

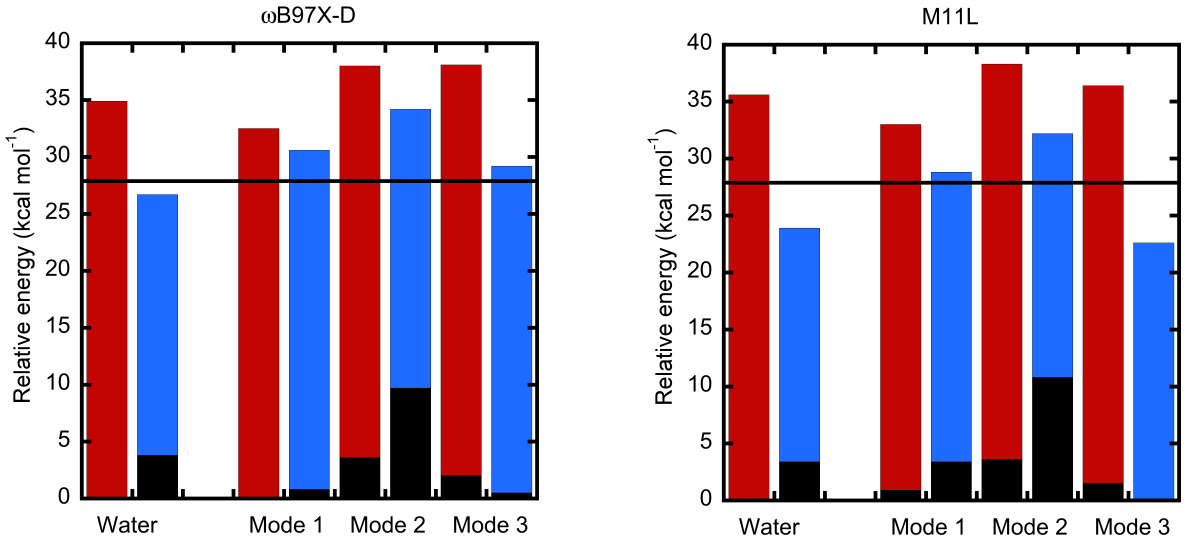

Figure 3: A comparison of the calculated and experimental activation free energies ($\Delta G^{\ddagger}$) for methyl triphosphate hydrolysis, obtained using the (left) ωB97X-D and (right) M11L functionals. The solid line indicates the experimental data ($\Delta G^{\ddagger}$ = 27.9 kcal·mol^{-1}). Black bars: the variation in the ground-state energy relative to the lowest energy calculated ground state (see the Methodology section). The red bars show the transition state energy for the substrate-assisted pathway, the blue bars show the transition state energy for the solvent-assisted pathway.

These show the lowest energy transition states obtained using the two different optimization strategies described in the Methodology section. In the case of the ωB97X-D functional, the energies of all relevant transition states, obtained either through direct optimization or through cross-optimization with the M11L functional, are shown in **Tables S1** and **S2** of the **Supporting Information**. In the case of MeTP complexed with Mg^{2+}, we used a single reference state, which was the lowest energy reactant state over all the Mg^{2+} binding modes we considered. Here, **Mode 1** corresponds to the Mg^{2+} ion coordinating the β- and γ-phosphates, **Mode 2** corresponds to Mg^{2+} ion coordinating the α- and β- phosphates (such that the primary role of the metal is leaving group stabilization), and **Mode 3** corresponds to the Mg^{2+} ion coordinating all three phosphates at once. For clarity, a schematic description of these three different Modes is also shown in **Figure 2**.

We note that in the case of the ωB97X-D functional, the lowest energy ground state we obtain is **Mode 1**, in which the metal ion bridges the β- and γ-phosphates. This has also been suggested to be the preferred binding mode in aqueous solution, and appears to be the preferred binding mode to GTP seen in the active sites of many GTPases (see, for example, refs. [16, 53-55], among others). In the case of the M11L functional, this shifts to **Mode 3**, however, for both functionals, the ground states for **Mode 1** and **Mode 3** are less than 1 $kcal \cdot mol^{-1}$ apart in energy, so they are essentially indistinguishable. In addition, and in contrast to some previous computational studies which suggested the presence of both phosphorane and metaphosphate-like intermediates [36, 37, 40], we obtain only transition states corresponding to concerted phosphoryl transfer processes, in line with our previous work on the hydrolysis of phosphate monoester dianions [19,20].

As can be seen from **Tables 1** and **2**, our calculated energetics for the lowest energy transition states for MeTP hydrolysis both with and without the presence of the Mg^{2+} ion are sensitive to the functional used. That is, in the case of the ωB97X-D functional, while we obtain reasonable agreement with experiment for our calculations without the metal ion present, once the Mg^{2+} ion is included in the system, this functional *overestimates* the calculated activation free energies compared to the experimentally observed value of 27.9 $kcal \cdot mol^{-1}$ at 25 °C. In contrast, the M11L functional *underestimates* the calculated activation free energies compared to experiment for calculations both with and without the Mg^{2+} present. However, the *trend* in reactivity between the different pathways and Mg^{2+} binding modes remains generally consistent between the two functionals. These variations highlight that care needs to be taken when considering the absolute energetics with different functionals, and suggests caution in interpreting the effect on Mg^{2+} on reactivity in too much

detail, as quantitative agreement with experiment may be merely coincidental. However, the experimentally observed effect on the reaction rates of saturating the substrate with Mg^{2+} is very small [34, 35] and consistent with our calculations: there is no large change in reactivity through coordination with Mg^{2+}. Relative to the activation energy calculated in the presence of only water, inclusion of the Mg^{2+} is slightly anti-catalytic when modeling the reaction using ωB97X-D, and slightly catalytic when modeling the reaction using M11L.

The effect of the metal ion on the discrimination between the solvent- and substrate-assisted pathways for the two systems can be interrogated with more confidence as these are internally consistent. While it is impossible to fully eliminate differences in energy between the two functionals due to slight differences in the positioning of the water molecules, we have aimed to minimize this by including the additional cross-optimization step between the different functionals described in the **Methodology** section. In doing so, we observe that the position of the nucleophile, Mg^{2+} and substrate at the transition state remains virtually identical independent of the optimization strategy used. However, in the case of the substrate-assisted pathway, shifts in the positions of these water molecules (which can change the hydrogen bonding patterns involved) can change the transition state energies by up to ~4 kcal·mol^{-1}, and this needs to be taken into account when comparing the energies of the different pathways for each system. Note that the solvent-assisted pathway appears to be far less sensitive to this – the differences in the substrate assisted pathway are mainly caused by movements of the proton on the phosphate at the transition state, which in turn changes the hydrogen bonding pattern of the water molecules.

It can be seen that for MeTP hydrolysis in the absence of the Mg^{2+} ion, the solvent-assisted pathway is clearly preferred over the substrate-assisted pathway by between 8 (ωB97X-D) and 12 (M11L) kcal·mol^{-1}. In both cases, the calculated activation free energy for the solvent-assisted pathway is in better agreement with the experimental value of 27.9 kcal·mol^{-1} [35] than the corresponding substrate-assisted pathway, although M11L appears to greatly underestimate the calculated activation free energy. This discrimination in favour of the solvent-assisted pathway still exists upon inclusion of the Mg^{2+} ion, regardless of the binding mode. Although the two functionals give quantitatively different results, the qualitative trends are similar, with the lowest energy transition state corresponding to the solvent-assisted pathway with the Mg^{2+} ion bound in **Mode 3**, and the trend **Mode 3** < **Mode 1** < **Mode 2** (although Mode 1 and 3 are similar in energy for the ωB97X-D functional, and the energy difference between all three modes is much smaller for ωB97X-D than for M11L). For the substrate-assisted pathway, both functionals show a clear preference for **Mode 1**, with

Modes 2 and **3** being either virtually identical in energy (ωB97X-D), or **Mode 2** being slightly higher than **Mode 3** (M11L). The overall magnitude of the discrimination is also much larger with the M11L functional than with the ωB97X-D functional when comparing the lowest energy transition states. Therefore, as with our recent work [20], we cannot with confidence establish how quantitatively unfavorable the substrate assisted-pathway is relative the solvent-assisted pathway, but our calculations suggest that it can be higher in energy than the solvent-assisted pathway by as much as 10 kcal·mol^{-1}, depending on the functional, when comparing the lowest energy modes for each pathway.

Table 1: A comparison of the activation free energies ($\Delta G^{\ddagger}$) of the substrate- and solvent-assisted hydrolyses of methyl triphosphate (MeTP) and acetyl phosphate (AcP) in aqueous solution, both in the presence and absence of an Mg^{2+} ion. All calculations were performed using the ωB97X-D functional[(a)].

System	Substrate-Assisted	Solvent-Assisted	Experiment
Methyl Triphosphate (MeTP)			
MeTP + H_2O	34.9	**26.7**	27.9[(b)]
MeTP•Mg^{2+} + H_2O (Mode 1)	32.5	30.6	27.9[(b)]
MeTP•Mg^{2+} + H_2O (Mode 2)	38.0	34.2	
MeTP•Mg^{2+} + H_2O (Mode 3)	38.1	**29.2**	
Acetyl Phosphate (AcP)			
AcP + H_2O	31.3	23.9	24.3[(c)]
AcP•Mg^{2+} + H_2O	31.4	**15.3**	23.9[(c)]

(a) All energies are in kcal·mol^{-1}, and the calculated values were obtained at the SMD-ωB97X-D/6-311++G(d,p)//SMD-ωB97X-D/6-31+G(d) level of theory for the electronic energies, and the SMD-ωB97X-D/6-31+G(d) level of theory for the zero point energies and entropies. Shown here are only the energies of the lowest energy transition states relative to the energy of the lowest energy reactant state obtained using the two different optimization strategies outlined in the **Methodology** section, in order to be able to directly compare the different relevant transition states against a common reference point. The relative energies of all structures are presented in **Tables S1** and **S2** of the **Supporting Information**, and the lowest energy transition state for each system is highlighted in bold. For a definition of **Modes 1-3**, see **Figure 2** and the main text.

(b) Values both with and without Mg^{2+} were obtained from ref. [35] (at 25 °C).

(c) Values both with and without Mg2+ were obtained from refs. [28, 29, 31-33] (experimental data was obtained at 39 °C in the absence of the metal ion, and 25 °C in the presence of the metal ion).

Table 2: A comparison of the activation free energies ($\Delta G^{\ddagger}$) of the substrate- and solvent-assisted hydrolyses of methyl triphosphate (MeTP) and acetyl phosphate (AcP) in aqueous solution, both in the presence and absence of an Mg^{2+} ion. All calculations were performed using the M11L functional[(a)].

System	Substrate-Assisted	Solvent-Assisted	Experiment
Methyl Triphosphate (MeTP)			
MeTP + H_2O	35.6	**23.9**	27.9[(b)]
MeTP•Mg^{2+} + H_2O (Mode 1)	33.0	28.8	27.9[(b)]
MeTP•Mg^{2+} + H_2O (Mode 2)	38.3	32.2	
MeTP•Mg^{2+} + H_2O (Mode 3)	36.4	**22.6**	
Acetyl Phosphate (AcP)			
AcP + H_2O	31.2	21.9	24.3[(c)]
AcP•Mg^{2+} + H_2O	32.2	**13.4**	23.9[(c)]

(a) All energies are in kcal·mol^{-1}, and the calculated values were obtained at the SMD-M11L/6-311++G(d,p)//M11L/6-31+G(d) level of theory for the electronic energies, and the SMD-M11L/6-31+G(d) level of theory for the zero point energies and entropies. For a definition of **Modes 1-3**, see **Figure 2** and the main text.

(b) Values both with and without Mg^{2+} were obtained from ref. [35] (at 25 °C).

(c) Values both with and without Mg^{2+} were obtained from refs. [28, 29, 31-33] (experimental data was obtained at 39 °C in the absence of the metal ion, and 25 °C in the presence of the metal ion).

From the data shown in **Tables 1** and **2**, it appears that coordination to Mg^{2+} is unable to lower the energies of the substrate-assisted pathways with different binding modes below those of the corresponding the solvent assisted pathways, and so the discrimination observed in the absence of Mg^{2+} remains, although it is quantitatively smaller than in the absence of the Mg^{2+} ion. In particular, we obtain substantially lower activation free energies using the M11L functional than previous computational studies, which obtained values that are typically [36, 38-40, 42, 43] in the range of 29-35 kcal·mol^{-1} (although lower values have also been reported [37, 41]). We note also that the **Mode 2** positions the Mg^{2+} to stabilize the leaving group, and avoids direct interactions with the terminal phosphate that is transferred. This might be expected to be the most favourable arrangement as it avoids introducing interactions between the cation and the metaphosphate-like (electron deficient) phosphoryl group. Indeed, comparing the energy difference between the ground state and the transition state for **Modes 2** and **3**, we note that **Mode 2** has a similar or smaller energy change. However, this is outweighed by the substantial difference in ground state energies, and so **Mode 3** is the preferred pathway. It appears that the change in the interactions with Mg^{2+} of the transferring phosphate are in the expected direction (*i.e.* presumably anticatalytic), but relatively minor.

The geometries of the relevant transition states calculated using the ωB97X-D functional are shown in **Figure 4)** and those calculated using the M11L functional are shown in **Figure S1** for comparison (these structures correspond to the transition states shown in **Tables 1** and **2**; coordinates for all transition states can be found as **Supporting Information**). The corresponding bond orders and bond distances to the incoming nucleophile and departing leaving group are shown in **Tables 3** and **5** for the ωB97X-D functional, and **Tables 4** and **6** for the M11L functional. The bond distances/bond orders corresponding to those of the lowest free energy transition state are highlighted in bold in all tables. As can be seen from this table, in the case of the substrate-assisted transition state, there is some bond formation to the nucleophile (~0.2) with more advanced bond cleavage to the leaving group (~0.5), in good agreement with our previous studies of phosphate monoesters [19, 20], but similarly also to the transition states we have obtained for hydroxide attack on phosphate diesters [56], fluorophosphates [57] and sulfonate monoesters [58]. Inclusion of the Mg^{2+} ion appears to have minimal effect on the transition state geometry. This is also the case for the solvent-assisted pathway, where the reaction proceeds through a loose dissociative transition state in aqueous solution, which is made slightly tighter by the inclusion of the Mg^{2+} ion (in all binding modes), but nevertheless still retains its overall dissociative character (bond orders of <0.2 and <0.1 to the nucleophile and leaving group respectively). Therefore, in all cases, the preferred transition state has very advanced bond cleavage to the leaving group, with minimal bond formation to the nucleophile, and only small changes in these parameters when the Mg^{2+} ion is present. Consistent with the discussion above, **Mode 2** resembles the solution more closely, with greater bond cleavage and reduced bond formation to the nucleophile than in **Modes 1** and **3**. In these latter modes, the structural effect of coordinating the transferring phosphoryl to Mg^{2+} is noticeable but not dramatic. This is in agreement with experimental studies of metallophosphatases such as alkaline phosphatase, where consideration of linear free energy relationships and substituent effects have suggested that the inclusion of positive charge in the active site has minimal effect on the nature of the transition states involved, although the energy does vary [59, 60].

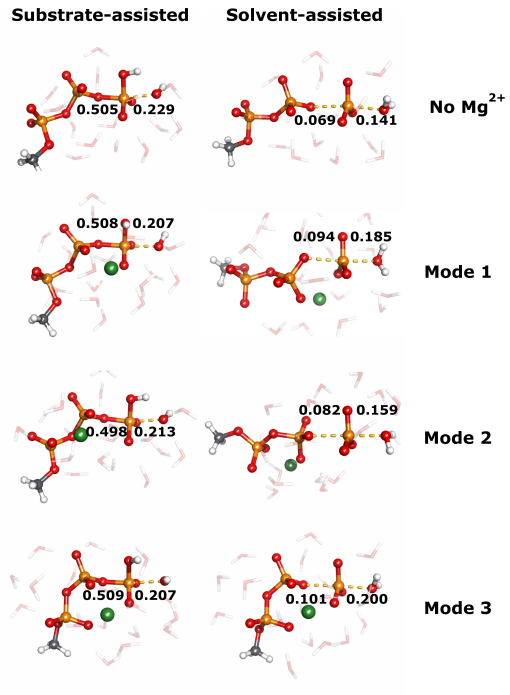

Figure 4: Geometries of the lowest energy transition states for the substrate- and solvent-assisted hydrolyses of methyl triphosphate in aqueous solution, optimized using the ωB97X-D functional, obtained as described in the Methodology section. The calculated bond orders to the incoming nucleophile and departing leaving group are also shown.

Table 3: Overview of calculated P-O_{lg} and P-O_{nuc} distances to the incoming nucleophile and departing leaving group respectively, at the transition states for the solvent- and substrate-assisted hydrolyses of methyl triphosphate (MeTP) and acetyl phosphate (AcP). All calculations were performed using the ωB97X-D functional [(a)].

System	Substrate-Assisted		Solvent-Assisted	
	P-O_{lg}	**P-O_{nuc}**	**P-O_{lg}**	**P-O_{nuc}**
Methyl Triphosphate (MeTP)				
MeTP + H_2O	1.74	2.18	**2.53**	**2.29**
MeTP•Mg^{2+} + H_2O (Mode 1)	1.73	2.22	2.42	2.19
MeTP•Mg^{2+} + H_2O (Mode 2)	1.74	2.22	2.47	2.25
MeTP•Mg^{2+} + H_2O (Mode 3)	1.73	2.26	2.39	2.17
Acetyl phosphate (AcP)				
AcP + H_2O	1.76	2.25	2.48	2.26
AcP•Mg^{2+} + H_2O	1.77	2.40	**2.39**	**2.23**

(a) All distances are in Å, and the calculated values were obtained at the SMD-ωB97X-D/6-31+G(d) level of theory, and correspond to the lowest energy transition states shown in **Table 1**. For an overview of all transition states obtained using the two different optimization strategies outlined in the **Methodology** section, see **Tables S3** and **S4** of the Supporting Information. For a definition of **Modes 1-3**, see **Figure 2** and the main text.

Table 4: Overview of calculated P-O_{lg} and P-O_{nuc} distances to the incoming nucleophile and departing leaving group respectively, at the transition states for the solvent- and substrate-assisted hydrolyses of methyl triphosphate (MeTP) and acetyl phosphate (AcP). All calculations were performed using the M11L functional[(a)].

System	Substrate-Assisted		Solvent-Assisted	
	P-O_{lg}	**P-O_{nuc}**	**P-O_{lg}**	**P-O_{nuc}**
Methyl Triphosphate (MeTP)				
MeTP + H_2O	1.72	2.12	**2.66**	**2.20**
MeTP•Mg^{2+} + H_2O (Mode 1)	1.70	2.14	2.48	2.18
MeTP•Mg^{2+} + H_2O (Mode 2)	1.71	2.15	2.56	2.20
MeTP•Mg^{2+} + H_2O (Mode 3)	1.69	2.18	**2.44**	**2.20**
Acetyl phosphate (AcP)				
AcP + H_2O	1.73	2.22	2.59	2.25
AcP•Mg^{2+} + H_2O	1.74	2.28	2.46	2.23

(a) All distances are in Å, and the calculated values were obtained at the SMD-M11L/6-31+G(d) level of theory. For a definition of **Modes 1-3**, see **Figure 2** and the main text.

Table 5: Overview of calculated P-O_{lg} and P-O_{nuc} bond orders to the incoming nucleophile and departing leaving group respectively, at the transition states for the solvent- and substrate-assisted hydrolyses of methyl triphosphate (MeTP) and acetyl phosphate (AcP). All calculations were performed using the ωB97X-D functional[(a)].

System	Substrate-Assisted		Solvent-Assisted	
	P-O_{lg}	**P-O_{nuc}**	**P-O_{lg}**	**P-O_{nuc}**
Methyl Triphosphate (MeTP)				
MeTP + H_2O	0.505	0.229	**0.069**	**0.141**
MeTP•Mg^{2+} + H_2O (Mode 1)	0.508	0.207	0.094	0.185
MeTP•Mg^{2+} + H_2O (Mode 2)	0.498	0.213	0.082	0.159
MeTP•Mg^{2+} + H_2O (Mode 3)	0.509	0.207	**0.101**	**0.200**
Acetyl phosphate (AcP)				
AcP + H_2O	0.491	0.173	0.088	0.158
AcP•Mg^{2+} + H_2O	0.471	0.138	0.101	0.164

(a) Bond orders were obtained from Wiberg bond indices [49] by performing natural bond orbital analysis [50] at the SMD-ωB97X-D/6-311++G(d,p) level of theory. For an overview of all transition states obtained using the two different optimization strategies outlined in the **Methodology** section, see **Tables S5** and **S6** of the Supporting Information For a definition of **Modes 1-3**, see **Figure 2** and the main text.

Table 6: Overview of calculated P-O_{lg} and P-O_{nuc} bond orders to the incoming nucleophile and departing leaving group respectively, at the transition states for the solvent- and substrate-assisted hydrolyses of methyl triphosphate (MeTP) and acetyl phosphate (AcP). All calculations were performed using the M11L functional[(a)].

System	Substrate-Assisted		Solvent-Assisted	
	P-O_{lg}	**P-O_{nuc}**	**P-O_{lg}**	**P-O_{nuc}**
Methyl Triphosphate (MeTP)				
MeTP + H_2O	0.460	0.226	**0.034**	**0.144**
MeTP•Mg^{2+} + H_2O (Mode 1)	0.475	0.207	0.058	0.153
MeTP•Mg^{2+} + H_2O (Mode 2)	0.464	0.210	0.045	0.142
MeTP•Mg^{2+} + H_2O (Mode 3)	0.481	0.202	**0.062**	**0.147**
Acetyl phosphate (AcP)				
AcP + H_2O	0.457	0.179	0.047	0.125
AcP•Mg^{2+} + H_2O	0.439	0.164	0.059	0.130

(a) Bond orders were obtained from Wiberg bond indices [49] by performing natural bond orbital analysis [50] at the SMD-ωB97X-D/6-311++G(d,p) level of theory. For a definition of Modes 1-3, see **Figure 2** and the main text.

Acetyl Phosphate Hydrolysis

We demonstrated in our recent study of phosphate monoester dianion hydrolysis that the better the leaving group, the larger the discrimination between the solvent- and substrate-assisted pathways (in favour of the solvent-assisted pathway) [20]. For comparison purposes, we have also considered here the impact of Mg^{2+} ions on the hydrolysis of acetyl phosphate which has a better leaving group than methyl triphosphate, and could be expected to show greater discrimination between the substrate- and solvent-assisted pathways.

Conveniently, acetyl phosphate hydrolysis is a well-studied reaction for which extensive experimental data exists [28, 29]. Specifically, the spontaneous hydrolysis of acetyl phosphate at 39 °C has a rate constant of 6.5×10^{-5} s^{-1} [28], corresponding to an activation barrier of 24.3 kcal·mol^{-1}, and is insensitive to nucleophilic or general base catalysis [29]. The effect of Mg^{2+} ions on the rate of hydrolysis of acetyl phosphate [28] and the binding constants for acetyl phosphate complexation with Mg^{2+} have also been studied. In both cases, the site of cleavage is the P-O bond [31]. An examination of the literature shows that the binding constants for Mg^{2+} to acetyl phosphate lie in the range of 6-75 M^{-1} from various reports [31-33], and are sensitive to the conditions under which the measurements have been made. Using a value of 10 M^{-1} gives a rate constant of 2.3×10^{-5} s^{-1} at 25 °C for this complex reacting with

water, compared with a value of 1×10^{-5} s^{-1} for acetyl phosphate reacting with water [32], and thus the effect of the Mg^{2+} on the overall reaction energetics is small, similar to the corresponding experimental observations for GTP [35] and ATP [34] hydrolysis. Additionally, from examining the effects of Mg^{2+} coordination on ATP and ADP [61], one can estimate that the effect of Mg^{2+} coordination to acetyl phosphate will be to lower its pK_a by about two units compared to free acetyl phosphate. Thus, the phosphoryl oxygen will be rather less basic than in a free phosphate.

Following from this, our calculations show that similar to methyl triphosphate hydrolysis, in the case of acetyl phosphate hydrolysis, we obtain again a large discrimination between the two pathways (**Tables 1 and 2**), with a predicted energy difference of up to ~9 kcal·mol^{-1} in the absence of the Mg^{2+} ion, compared with up to 12 kcal·mol^{-1} in the case of methyl triphosphate hydrolysis. In addition, the calculated $\Delta G^{\ddagger}$ of 23.9 kcal·mol^{-1} with the ωB97X-D functional is in good agreement with the experimental value (24.3 kcal·mol^{-1}) [28], and, again, M11L slightly underestimates the activation free energy, as with MeTP. In contrast to MeTP hydrolysis, however, the effect of including the metal ion is now quite radical on the calculated energetics of the solvent-assisted pathway, reducing the energies of the solvent assisted pathway by ~8.5 kcal·mol^{-1}. This over-exaggeration is likely a simulation artifact akin to the corresponding problems observed when performing calculations with the hydroxide ion (see discussion in refs. [58, 62] and references cited therein), and, interestingly, the energetics of the corresponding substrate-assisted pathway appear to be minimally affected by inclusion of the metal ion. However, it does appear to be clear that the metal ion (now with only one binding mode) creates a significant difference between the substrate- and solvent-assisted pathways, with the solvent-assisted pathway being preferred over the solvent-assisted pathway by up to ~19 kcal·mol^{-1} depending on functional.

It seems likely that inclusion of the metal ion amplifies the discrimination between the two pathways due to the fact that complexation to the metal ion reduces the pK_a of the non-bridging oxygens of the phosphate making them poorer proton acceptors (note that, as can be seen from **Figure 5**, in the solvent-assisted pathway, the nucleophile is not yet deprotonated at the highly dissociative transition state, and is thus less affected by metal-induced pK_a changes). It is comforting, however, that despite quantitative differences, the qualitative trends for both substrates can be reproduced by both the functionals considered in this work, thus further increasing our confidence in our qualitative conclusions about the structural and energetic effects of the inclusion of Mg^{2+} on the competition between the two pathways.

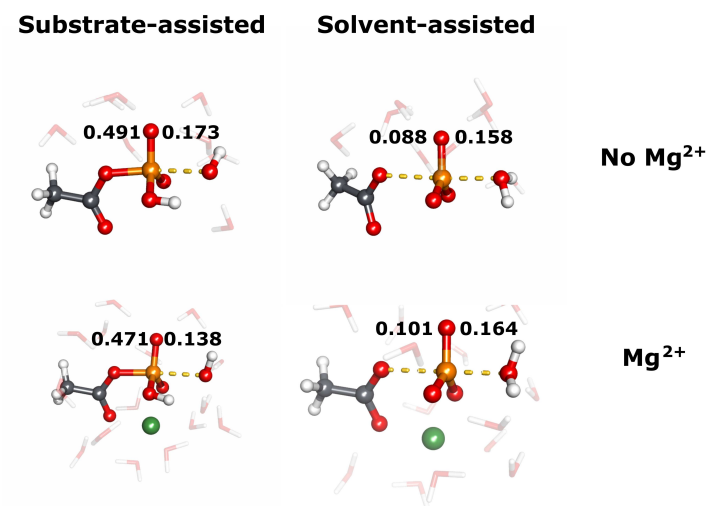

Figure 5: Geometries of the lowest energy transition states for the substrate- and solvent-assisted hydrolyses of acetyl phosphate in aqueous solution, optimized using the ωB97X-D functional, obtained as described in the Methodology section. The calculated bond orders to the incoming nucleophile and departing leaving group are also shown.

Conclusions

We have examined here the effect of Mg^{2+} on the energetic and geometries of the substrate- and solvent-assisted hydrolyses of methyl triphosphate and acetyl phosphate. We propose a preferred binding mode involving all three phosphate groups for methyl triphosphate hydrolysis, and demonstrate that the transition state geometries remain largely unchanged by inclusion of the metal ion. These calculations do not explicitly rule out a substrate-assisted mechanism as a potential solution for catalyzing the hydrolysis of phosphate monoesters with good leaving groups by metallophosphatases, and the differences we observed between the two functionals emphasize the importance of not drawing conclusions based on a single functional but rather comparing results using different levels of theory. They do, however, demonstrate that a substantial additional energetic cost would need to be overcome for this to be a viable mechanism. The more expansive, solvent-assisted pathway is clearly energetically preferred, both with and without Mg^{2+} present. We note here that one potential caveat of these calculations is the risk of having become trapped in a local metastable arrangement of water molecules, although, as outlined in the Methodology section, we have taken great care to keep the water arrangements as consistent as possible, both in between pathways, and in between functionals. In addition, as we have demonstrated earlier, the larger the number of water molecules included in the calculations, the less likely this is to be a problem as changes in water arrangement start disappearing in the general noise of the

calculations [19]. Therefore, based on these data, it is highly unlikely that a substrate-assisted pathway is, *a priori*, a preferred mechanism for metallophosphatases that catalyze the hydrolysis of phosphate esters with good leaving groups, such as Ras GTPase and related enzymes.

Acknowledgments

The European Research Council has provided financial support under the European Community's Seventh Framework Programme (FP7/2007-2013)/ERC Grant Agreement No. 306474. The Knut and Alice Wallenberg Foundation has provided financial support through a Wallenberg Academy Fellowship to S. C. L. K. Finally, we are grateful to the Swedish National Infrastructure for Computing (SNIC, 2015/16-12) for their generous provision of computational resources.

References

1. F. H. Westheimer. *Science* **235**, 1173-1178 (1987).
2. W. W. Cleland, A. C. Hengge. *Chem. Rev.* **106**, 3252-3278 (2006).
3. P. Cohen. *Nat. Rev. Drug Discov.* **1**, 309-315 (2002).
4. S. Zhang, Z. Y. Zhang. *Drug Discov. Today* **12**, 373-381 (2007).
5. A. J. Barr. *Future Med. Chem.* **2**, 1563-1576 (2010).
6. J. K. Lassila, J. G. Zalatan, D. Herschlag. *Annu. Rev. Biochem.* **80**, 669-702 (2011).
7. S. C. L. Kamerlin, P. K. Sharma, R. B. Prasad, A. Warshel. *Q. Rev. Biophys.* **46**, 1-132 (2013).
8. A. T. P. Carvalho, K. Szeler, K. Vavitsas, J. Aqvist, S. C. L. Kamerlin. *Arch. Biochem. Biophys.* **582**, 80-90 (2015).
9. T. Schweins, M. Geyer, K. Scheffzek, A. Warshel, H. R. Kalbitzer, A. Wittinghofer. *Nat. Struct. Biol.* **2**, 36-44 (1995).
10. S. Pasqualato, J. Cherfils. *Structure* **13**, 533-540 (2005).
11. C. Kötting, M. Blessenohl, Y. Suveyzdis, R. S. Goody, A. Wittinghofer, K. Gerwert. *Proc. Natl. Acad. Sci. USA* **103**, 13911-13916 (2006).
12. A. J. Adamczyk, A. Warshel. *Proc. Natl. Acad. Sci. USA* **108**, 9827-9832 (2011).
13. G. Wallin, S. C. L. Kamerlin, J. Åqvist. *Nat. Commun.* **4** (2013).

14. U. Krengel, I. Schlichting, A. Scherer, R. Schumann, M. Frech, J. John, W. Kabsch, E. F. Pai, A. Wittinghofer. *Cell* **62**, 539-548 (1990).

15. E. F. Pai, U. Krengel, G. A. Petsko, R. S. Goody, W. Kabsch, A. Wittinghofer. *EMBO J.* **9**, 2351-2359 (1990).

16. R. M. Voorhees, T. M. Schmeing, A. C. Kelley, V. Ramakrishnan. *Science* **330**, 835-838 (2010).

17. M. G. Khrenova, B. L. Grigorenko, A. B. Kolomeisky, A. V. Nemukhin. *J. Phys. Chem. B* **119**, 12838-12845 (2015).

18. Y. Jin, R. W. Molt Jr., J. P. Waltho, N. G. J. Richards, G. M. Blackburn. *Angew. Chem. Int. Ed.* **55**, 3318-3322 (2016).

19. F. Duarte, J. Åqvist, N. H. Williams, S. C. L. Kamerlin. *J. Am. Chem. Soc.* **137**, 1081-1093 (2015).

20. F. Duarte, A. Barrozo, J. Åqvist, N. H. Williams, S. C. L. Kamerlin. *J. Am. Chem. Soc.* **138**, 10664-10673 (2016).

21. A. J. Kirby, W. P. Jencks. *J. Am. Chem. Soc.* **87**, 3209-3216 (1965).

22. A. J. Kirby, A. G. Varvoglis. *J. Am. Chem. Soc.* **89**, 415-423 (1967).

23. A. J. Kirby, A. G. Varvoglis. *J. Chem. Soc. B*, 135-141 (1968).

24. A. C. Hengge, W. A. Edens, H. Elsing. *J. Am. Chem. Soc.* **116**, 5045-5049 (1994).

25. M. F. Mohamed, F. Hollfelder. *Biochim. Biophys. Acta* **1834**, 417-424 (2013).

26. F. Baier, J. Chen, M. Solomonson, N. C. Strynadka, N. Tokuriki. *ACS Chem. Biol.* **10**, 1684-1693 (2015).

27. F. Lipmann, L. C. Tuttle. *Arch. Biochem.* **13**, 373-377 (1947).

28. D. E. Koshland Jr. *J. Am. Chem. Soc.* **74**, 2286-2292 (1952).

29. G. Di Sabato, W. P. Jencks. *J. Am. Chem. Soc.* **83**, 4393-4400 (1961).

30. G. Di Sabato, W. P. Jencks. *J. Am. Chem. Soc.* **83**, 4400-4405 (1961).

31. C. H. Oestreich, M. M. Jones. *Biochemistry* **5**, 2926-2931 (1966).

32. P. J. Briggs, D. P. Satchell, G. F. White. *J. Chem. Soc. B*, 1008-1012 (1970).

33. R. Kluger, P. Wasserstein, K. Nakaoka. *J. Am. Chem. Soc.* **97**, 4298-4303 (1975).

34. S. J. Admiraal, D. Herschlag. *Chem. Biol.* **2**, 729-739 (1995).

35. C. Kötting, K. Gerwert. *Chem. Phys.* **307**, 227-232 (2004).

36. J. Akola, R. O. Jones. *J. Phys. Chem. B.* **107**, 11774-11783 (2003).

37. B. L. Grigorenko, A. V. Rogov, A. V. Nemukhin. *J. Phys. Chem. B* **110**, 4407-4412 (2006).

38. M. Klähn, E. Rosta, A. Warshel. *J. Am. Chem. Soc.* **128**, 15310-15323 (2006).

39. C. B. Harisson, K. Schulten. *J. Chem. Theory and Comput.* **8**, 2328-2335 (2012).

40. R. Glaves, G. Mathias, D. Marx. *J. Am. Chem. Soc.* **134**, 6995-7000 (2012).

41. N. V. Plotnikov, R. B. Prasad, S. Chakrabarty, Z. T. Chu, A. Warshel. *J. Phys. Chem. B* **117**, 12807-12819 (2013).

42. C. Wang, W. Huang, J.-L. Liao. *J. Phys. Chem. B* **119**, 3720-3726 (2015).

43. R. Tripathi, R. Glaves, D. Marx. *Chem. Sci.* **Advance Article**, DOI: 10.1039/C1036SC02045C (2017).

44. W. J. Li, T. Rudack, K. Gerwert, F. Grater, J. Schlitter. *J. Chem. Theory Comput.* **8**, 3596-3604 (2012).

45. H. P. Hratchian, H. B. Schlegel. *J. Chem. Phys.* **120**, 9918-9924 (2004).

46. H. P. Hratchian, H. B. Schlegel. *J. Chem. Theory Comput.* **1**, 61-69 (2005).

47. J. D. Chai, M. Head-Gordon. *Phys. Chem. Chem. Phys.* **10**, 6615-6620 (2008).

48. A. V. Marenich, C. J. Cramer, D. G. Truhlar. *J. Phys. Chem. B* **113**, 6378-6396 (2009).

49. K. B. Wiberg. *Tetrahedron* **24**, 1083-1096 (1968).

50. J. P. Foster, F. Weinhold. *J. Am. Chem. Soc.* **102**, 7211-7218 (1980).

51. R. Peverati, D. G. Truhlar. *J. Phys. Chem. Lett.* **3**, 117-124 (2012).

52. M. J. Frisch, G. W. Trucks, H. B. Schlegel, G. E. Scuseria, M. A. Robb, J. R. Cheeseman, G. Scalmani, V. Barone, B. Mennucci, G. A. Petersson, H. Nakatsuji, M. Caricato, X. Li, H. P. Hratchian, A. F. Izmaylov, J. Bloino, G. Zheng, J. L. Sonnenberg, M. Hada, M. Ehara, K. Toyota, R. Fukuda, J. Hasegawa, M. Ishida, T. Nakajima, Y. Honda, O. Kitao, T. Nakai, T. Vreven, J. A. Montgomery Jr., J. E. Peralta, F. Ogliaro, M. Bearpark, J. J. Heyd, E. Brothers, K. N. Kudin, V. N. Staroverov, R. Kobayashi, J. Normand, K. Raghavachari, A. Rendell, J. C. Burant, S. S. Iyengar, J. Tomasi, M. Cossi, N. Rega, J. M. Millam, M. Klene, J. E. Knox, J. B. Cross, V. Bakken, C. Adamo, J. Jaramillo, R. Gomperts, R. E. Stratmann, O. Yazyev, A. J. Austrin, R. Cammi, C. Pomelli, J. W. Ochterski, R. L. Martin, K. Morokuma, V. G. Zakrzewski, G. A. Voth, P. Salvador, J. J. Dannenberg, S. Dapprich, A. D. Daniels, Ö. Farkas, J. B. Foresman, J. V. Ortiz, J. Cioslowski, D. J. Fox. *Gaussian 09, Revision E.01*, Gaussian Inc., Wallingford CT.

53. A. J. Scheidig, C. Burmester, R. S. Goody. *Structure Fold. Des.* **7**, 1311-1324 (1999).

54. K. Scheffzek, M. R. Ahmadian, W. Kabsch, L. Wiesmuller, A. Lautwein, F. Schmitz, A. Wittinghofer. *Science* **277**, 333-338 (1997).

55. E. M. Gazdag, K. Gavriljuk, A. Itzen, C. Koetting, K. Gerwert, R. S. Goody. *Proc. Natl. Acad. Sci. USA* **109**, 21348-21353 (2012).

56. E. Rosta, S. C. L. Kamerlin, A. Warshel. *Biochemistry* **47**, 3725-3735 (2008).

57. A. Alkherraz, S. C. L. Kamerlin, G. Feng, Q. I. Sheikh, A. Warshel, N. H. Williams. *Faraday Discuss.* **145**, 281-299 (2010).

58. F. Duarte, T. Geng, G. Marloie, A. O. Al Hussain, N. H. Williams, S. C. L. Kamerlin. *J. Org. Chem.* **79**, 2816-2828 (2014).

59. I. Nikolic-Hughes, D. C. Rees, D. Herschlag. *J. Am. Chem. Soc.* **126**, 11814-11819 (2004).

60. J. G. Zalatan, D. Herschlag. *J. Am. Chem. Soc.* **128**, 1293-1303 (2006).

61. V. L. Pecoraro, J. D. Hermes, W. W. Cleland. *Biochemistry* **23**, 5262-5271 (1984).

62. F. Duarte, S. Gronert, S. C. L. Kamerlin. *J. Org. Chem.* **79**, 1280-1288 (2014).